Materials Horizons

Photochemical Ligation Meets Nanocellulose: A Versatile Platform for Self-Reporting Functional Materials

Journal:	*Materials Horizons*
Manuscript ID	MH-COM-02-2018-000241.R1
Article Type:	Communication
Date Submitted by the Author:	05-Apr-2018

Complete List of Authors:	Hoenders, Daniel; University of Freiburg, Institute for Macromolecular Chemistry Guo, Jiaqi; Albert-Ludwigs-Universität Freiburg, Institute of Macromolecular Chemistry; Goldmann, Anja; Karlsruhe Institute of Technology, Institute of Chemical Technology and Polymer Chemistry; Queensland University of Technology Faculty of Science and Engineering, Barner-Kowollik, Christopher; Queensland Universtiy of Technology, School of Chemistry, Physics and Mechanical Engineering; Karlsruhe Institute of Technology, Institut für Technische Chemie und Polymerchemie Walther, Andreas; University of Freiburg, Institute for Macromolecular Chemistry

Photochemical Ligation Meets Nanocellulose: A Versatile Platform for Self-Reporting Functional Materials

Daniel Hoenders,[a] Jiaqi Guo,[a] Anja S. Goldmann,[b] Christopher Barner-Kowollik*[b] and Andreas Walther*[a]

[a] Institute for Macromolecular Chemistry, Albert-Ludwigs-University Freiburg, Stefan-Meier-Straße 31, 79104 Freiburg, Germany

Freiburg Materials Research Center, Albert-Ludwigs-University Freiburg, Stefan-Meier-Straße 21, 79104 Freiburg, Germany

Freiburg Center for Interactive Materials and Bioinspired Technologies, Albert-Ludwigs-University Freiburg, Georges-Köhler-Allee 105, 79110 Freiburg, Germany

Freiburg Institute for Advanced Studies (FRIAS), Albert-Ludwigs-University Freiburg, 79104 Freiburg, Albertstraße 19, 79104 Freiburg, Germany, andreas.walther@makro.uni-freiburg.de

[b] School of Chemistry, Physics and Mechanical Engineering, Queensland University of Technology (QUT), 2 George St, QLD 4000, Brisbane, Australia, christopher.barnerkowollik@qut.edu.au

Macromolecular Architectures, Institut für Technische Chemie und Polymerchemie, Karlsruhe Institute of Technology (KIT), Engesserstr. 18, 76128 Karlsruhe, Germany

Institut für Biologische Grenzflächen, Karlsruhe Institute of Technology (KIT), Hermann-von-Helmholtz-Platz 1, 76344, Eggenstein-Leopoldshafen, Germany, christopher.barner-kowollik@kit.edu

Conceptual insights

Cellulose nanofibrils (CNFs) are next generation, renewable building blocks for sustainable, high-performance bioinspired materials uniting high stiffness, strength and biocompatibility. In many CNF applications, it would be highly desirable to have freedom of controlling chemical functionality via simple and highly selective means. Photo-click reactions are the most capable ones to control spatiotemporal reactivity, and the UV-induced NITEC (tetrazole/maleimide) cycloaddition reaction is a very promising one, as it leads to fluorescent adduct allowing to monitor the reaction progress. Here, we provide a conceptual approach by merging for the first time CNFs with this highly selective and self-reporting photo-click reaction, which allows the spatiotemporal control of the chemical functionality with in-situ recording of the reaction progress by fluorescence. The relevance of combining these two independent disciplines – advanced photochemistry with sustainable nanocellulose – is highlighted by developing platform methods for different sustainable CNF material classes: (i) Photo-functional nanopaper surfaces for biosensors. (ii) Photo-induced hydrogels, and (iii) Photo-engineering of molecular energy dissipation mechanisms in bioinspired bulk nanocomposites.

Abstract

The sustainable origin and highly promising mechanical and functional properties of cellulose nanofibrils (CNFs) attract significant interest for the construction of advanced functional materials. One key aspect to promote functionality of CNF-based materials is to implement sophisticated, facile and versatile chemical functionalization principles for application-targeted modification of CNF properties, independent on whether aiming for functional surfaces, hydrogels or bulk materials. We herein merge for the first time a self-reporting photo-induced modular ligation, the UV-induced nitrile imine-mediated tetrazole/ene cycloaddition, with CNFs to control chemical functionality in space and time with the possibility for a macroscopic fluorescence readout of the reaction progress. We discuss this hetero-complimentary photo-conjugation with respect to immobilization of the photoactive tetrazole units on CNFs in bulk and dispersion, and demonstrate the application for the three important CNF-based material classes (surfaces, hydrogels and bioinspired nanocomposites) by modification with photo-complementary maleimide-tethered functional moieties. In addition to realizing selective biorecognition patterns on transparent nanopapers, we present photo-induced hydrogelation relevant for biomaterials, as well as mechanical stiffening in bioinspired nanocomposites in bulk. The photochemical ligation proceeds smoothly in all three materials of vastly different dynamics (solution to bulk) and hence establishes a platform methodology to promote self-reporting functionalization of diverse CNF-based materials.

Introduction

Cellulose nanofibrils (CNFs) have emerged as one of the most significant sustainable building blocks for the development of high-performance and functional materials.[1-3] The applications range from mechanically robust bioinspired films, nanocomposites and macrofibers to functional films and aerogel materials, fire-retardant foams and up to 3D-printed tissue engineering constructs using CNFs as fibrillar artificial extracellular matrix.[4-20] The outstanding mechanical performance of CNF-based materials originates from the crystalline domains of the underlying cellulose I (E = 140 GPa) and is influenced on a materials and systems level by surface charges, polymer additives, and humidity.[1, 21-31] In all of the above-mentioned applications, it is of crucial importance to achieve control over surface functionality and interactions with the surrounding to modulate the functional characteristics.

Nonetheless, sophisticated chemical modifications on CNFs remain a challenge, as those mostly need to be conducted in aqueous medium to preserve the nanofibrillar CNF structure and prevent irreversible agglomeration. Several methods for activation of cellulose surfaces by adsorption of tailored polymers or/and "click" chemistry are described in literature.[32-35] However, they lack in possibilities for spatiotemporal applications. Among various chemistries for surface modification of CNFs, one suitable starting point for further subsequent modification of CNFs is the introduction of carboxylate groups through carboxymethylation or 2,2,6,6-tetramethyl-1-peperidinyloxy (TEMPO)-mediated oxidation, typically used to facilitate the fibrillation process and provide colloidal stability by introducing interfibrillar electrostatic repulsion.[36-39] Recent publications demonstrated the heterogeneous modification of parent pulp or CNFs via carbodiimide-mediated amidation reactions to ultimately improve the mechanical properties of nanopapers, to confer hydrophobic character, or to immobilize peptides and proteins for applications in diagnostics.[40-43]

While such classical chemical reactions are valuable, it would be highly desirable to develop pathways for an on-demand control of chemical reactions and functionality in space and time. To this end, light-triggered, highly selective, hetero-complimentary photochemical reactions are of critical importance, as they constitute an emerging class of modular ligations, allowing in principal for a spatial, temporal and wavelength-based control over chemical functionalization.[44-46] One promising example of such photo-reactions is the photo-induced nitrile imine-mediated tetrazole/ene cycloaddition (NITEC), which generates a fluorescent and self-reporting pyrazoline cycloadduct for *in situ* monitoring of the conversion.[47-49] By the choice of the photochemically complementary dipolarophiles (typically maleimide

derivatives), the resulting cycloadduct can be tuned to suit functional needs. Moreover the reaction occurs free of any catalyst and under mild reaction conditions, providing bioorthogonality, and can be conducted even using two-photon excitation in confocal volumes in life cells, demonstrating highest spatiotemporal control.[50-52] Recent work demonstrated NITEC for modification of fully dissolved cellulose in organic media or for modification of paper, which both, however, fall short of the synthetic demands and application prospects of nanocellulose.[53-55] More conventional approaches for photochemical modifications of nanocellulose include non-specific benzophenone or self-complementary coumarin, which are limited to crosslinking purposes and cannot serve specific and controlled hetero-complementary modular ligation for functionalization with highest levels of control.[43, 56-58] Very recently, the photochemical modification of nanopaper surfaces using photo-mediated thiol-ene reactions (not self-reporting) was shown to, for instance, create superhydrophobic surfaces.[59] This demonstrates that advances are in reach using modern photochemistry in combination with nanocellulose, yet, the next level of control will be in reach by implementing self-reporting and highly selective photochemistries, as well as realizing modifications in bulk systems.

Herein, we fuse advanced self-reporting, modular, and hetero-complimentary ligation photochemistry with sustainable CNFs in different material states. We equip CNFs in dispersion and in bulk with tetrazole units and demonstrate their functionalization using photochemically complementary maleimide-carrying derivatives via NITEC. We focus on an elucidation of such a self-reporting functionalization platform for three of the most important classes of nanocellulose materials: Transparent nanopaper surfaces, hydrogels with tunable sol/gel transition and for the engineering of molecular energy dissipation mechanisms in bioinspired bulk CNF/polymer nanocomposites.

Results and Discussion

Our investigations start with the preparation of CNFs by TEMPO-mediated oxidation of wood pulp at neutral conditions resulting in a charge density of COOH/COONa groups of 0.94 mmol g^{-1}. Homogenization in a microfluidizer then liberates micrometer-long CNFs with diameters of 1 – 4 nm (Figure 1a). Subsequently, we first focus on the modification of the CNFs in dispersion (and later in bulk) as depicted in Scheme 1 and described below.

The main challenge for the functionalization of CNFs is to find solvent combinations that allow for a dissolution of often hydrophobic modifications allowing for their attachment, while at the same time preventing aggregation of the CNFs in increasingly non-polar solvents. In addition,

if hydrophobic modifications are tethered to the CNFs, their content should not be too high to prevent re-dispersion of modified CNFs in aqueous media needed for the design of many functional materials. Hence, a delicate balance between density of hydrophobic modifications and sufficient colloidal stability in different media needs to be found.

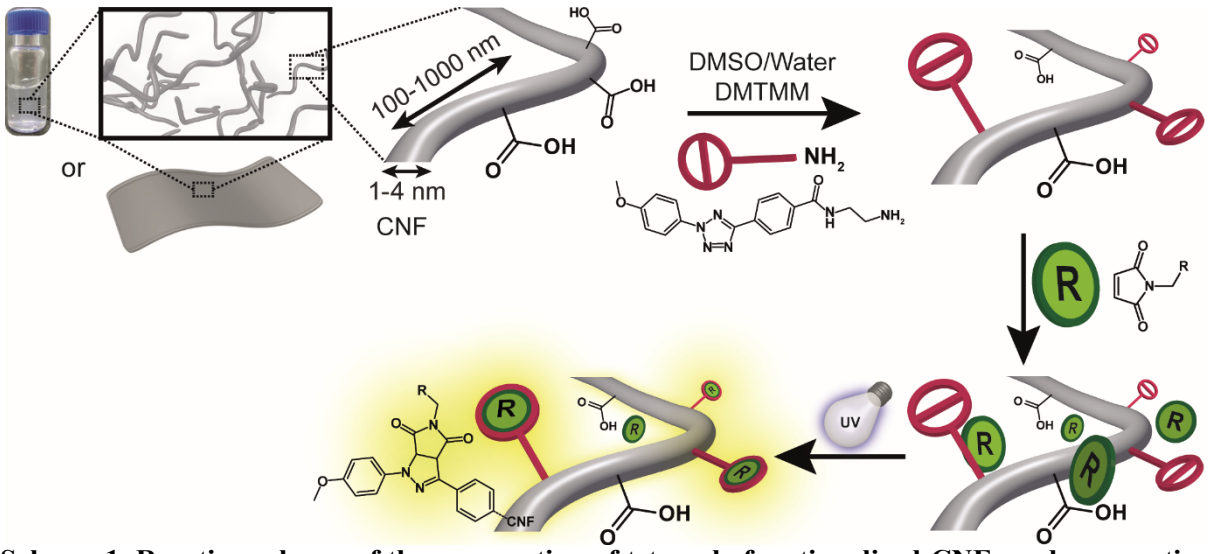

Scheme 1. Reaction scheme of the preparation of tetrazole-functionalized CNFs and consecutive functionalization with a maleimide-based compound using the NITEC reaction. Starting with CNFs, either modified in bulk or in dispersion with tetrazole-NH_2, the maleimide-modified functional compound can be covalently attached via NITEC reaction upon UV light irradiation of the tetrazole-functionalized CNFs.

Suitable approaches for the modification of hydrophilic CNFs with hydrophobic molecules proceed in aqueous mixtures of polar aprotic solvents like DMSO or DMF.[43, 60, 61] In our case, both the CNF as well as the tetrazole-NH_2 are sufficiently well dispersed and dissolved in water/DMSO (1/4 v/v), respectively, allowing for chemical attachment. Most water-based approaches for amide bond formation use carbodiimide-mediated activation of the carboxylic groups on the CNF surface with *N*-ethyl-*N*-(3-dimethylaminopropyl) carbodiimide (EDC) and *N*-hydroxysuccinimide (NHS). However, this method may not be ideally suited for CNFs, as we observed a considerable formation of a stable *N*-acylurea side product by rearrangement of the unstable *O*-acylisourea intermediate, which remains difficult to separate, and even feigns higher degrees of apparent modification in FTIR and elemental analysis than actually present (Figure SI1).[62, 63] Therefore, we changed to a rarely used coupling agent, 4-(4,6-dimethoxy-1,3,5-triazin-2-yl)-4-methylmorpholinium (DMTMM), which is known to be more efficient for amidation reactions on polysaccharides (e.g. on hyaluronic acid) compared to EDC/NHS.[64]

Additionally, DMTMM does not require a specific pH, and facilitates purification as potentially remaining, intermediate active esters (CNF-COO-DMTMM) hydrolyze during washing. To understand this reaction, we conducted the grafting of tetrazole-NH_2 onto (i) CNFs in water/DMSO (1/4 v/v) dispersion as well as in (ii) bulk films after swelling in water/DMSO (1/4 v/v) mixtures using a 3-4 fold excess of tetrazole-NH_2 and DMTMM with respect to the CNF carboxyl groups.

Fourier Transform Infrared Spectroscopy (FTIR) of freeze-dried tetrazole-modified CNFs (CNF-Tet, Figure 1c) dispersions (top) and films (bottom) confirms the successful amide bond formation for both routes. The spectra clearly display a decrease of the COOH/COO^--based bands (1725 cm^{-1} and 1645 cm^{-1}), while new peaks appear at 1552 cm^{-1} (combined C-N stretching and N-H deformation of amide II) and at 1512 cm^{-1} (C=C aromatic symmetrical stretching). The spectra of the control experiments (physical mixture of CNF and tetrazole-NH_2 without DMTMM; dotted lines) corroborate that the conjugation is covalent and persistent, as all tetrazole-NH_2 is removed during washing.

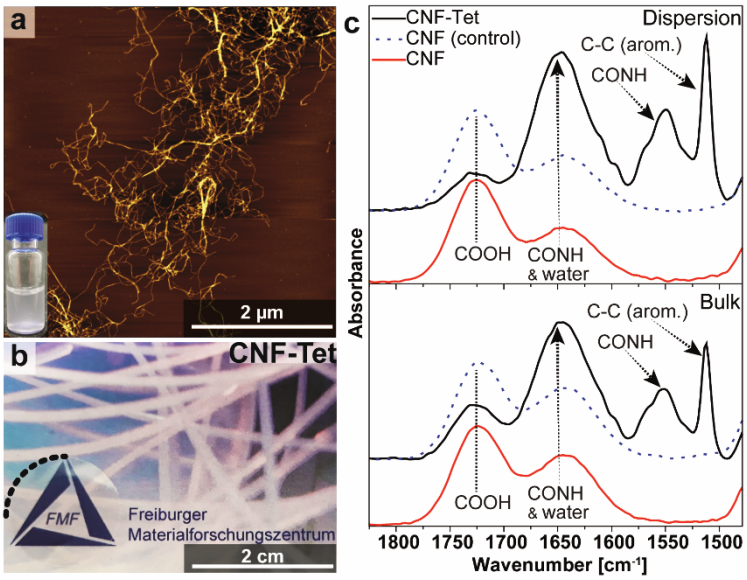

Figure 1. Characterization of tetrazole-functionalized CNFs (CNF-Tet): (a) AFM height image of CNF-Tet (z-scale = 5 nm; see Figure SI2 for non-modified CNF) and (b) translucent bulk film after modification (bottom left, black dashed line as a guide to the eyes). FTIR spectra (c) of freeze-dried dispersions under acidic condition (top) and film (bottom) of CNF-Tet (black) in comparison with non-modified CNF (red). The control CNF (dotted line) without addition of DMTMM is shown for comparison.

We further quantified the amount of bound tetrazole units via elemental analysis (see Table 1), revealing a slightly higher functionalization in bulk (0.36 mmol g^{-1}) compared to the reaction in dispersion (0.30 mmol g^{-1}). This corresponds to a modification of ca. 1/3 of the available COOH groups on the CNFs. Both controls, either not having DMTMM or tetrazole,

respectively, do not show a nitrogen content, confirming an efficient purification and that the nitrogen content indeed arises from covalently tethered tetrazole units. The AFM height image of the modified CNFs shows the characteristic fibrillar CNF structure (Figure 1a), and a 0.5 wt% dispersion of CNF-Tet in water remains stable for several months without sedimentation (Figure 1a, inset). This desirable stability in dispersion allows further modifications and proper film formation by solvent casting. It is assisted by maintaining a certain fraction of the COOH groups (here ca. 2/3) during the synthesis to ensure efficient electrostatic stabilization.

Table 1. Conditions for and characterization of modified CNFs with tetrazole-NH_2

Sample	Tet-NH_2 equiv. [a]	DMTMM equiv. [a]	N content (%) [b]	Tetrazole content (mmol g^{-1}) [c]	Conv. of COOH groups (mol%)
CNF	0	0	0	-	-
CNF-Tet (disp.)	3	4	2.6	0.30	32.3
CNF-Tet (bulk)	3	4	3.0	0.36	37.9
CNF (control I)	3	0	0	-	-
CNF (control II)	0	4	0	-	-

[a] Molar ratios in relation to carboxylic groups of CNF (0.94 mmol g^{-1}). [b] Determined by elemental analysis. [c] Calculated from nitrogen content.

As a basic proof of principle, we will first describe the patterning of biorecognition and antifouling areas on otherwise transparent CNF-Tet nanopapers (Figure 2, Figure 1b), which had been modified with the tetrazole units in bulk as described above. To this end, we designed a photomask using inkjet printing on a transparent foil, featuring eight black non-translucent bars with increasing spacings (from 155 µm (thinnest) to 575 µm (widest)). Biotin-DEG-maleimide (DEG = diethylene glycol) serves as a specific biorecognition compound for Avidin, while a longer chain PEG-maleimide (M_n = 750 Da) is used as surface modifier to impart protein-repellent behavior.[65] Both compounds can be sequentially immobilized in an alternating fashion by first putting one droplet of compound A onto the surface and subsequently irradiating the sample through the tightly attached photomask (30 min, λ = 305 nm, 6 mW cm^{-2}). After washing, compound B is added and linked to the previously non-exposed surface by irradiation under similar conditions. Figure 2 illustrates the process for one procedure.

The spatially selective activation of the tetrazole units and subsequent linkage to the maleimide-derivatives can be followed by confocal laser scanning microscopy (CLSM; Figure 2b) via the appearance of the self-reporting, fluorescent pyrazoline pattern. Evaluation of the width of the patterns by CLSM results in resolutions of 185 ± 5 µm (thinnest) and 595 ± 5 µm (widest), being, as expected slightly wider, than the 155 µm and 575 µm target width of the photomask, respectively. The following successful selective biorecognition on the biotin-modified areas

can be traced using Texas Red-modified Avidin, which selectively binds to the previously modified biotin areas, and which leads to the appearance of a strong red fluorescence in these areas (Figure 2c, d).

A comparison of the two strategies, either photo-patterning the biotin-DEG-maleimide or the PEG-maleimide (Figure 2 c, d), reveals a higher contrast for the surface selectively patterned with the biotin-DEG-maleimide units (Figure 2c). This indicates a slightly better localization and more selective protein immobilization following this strategy. This is not surprising, because the addition of biotin-DEG-maleimide in the second photo-conjugation step (unmasked) may lead to some additional immobilization to some unreacted groups in the previously photo-patterned areas. Overall, this demonstrates that transparent CNF nanopapers can be photo-patterned with functional, bioactive surface groups that can spatially selectively recognize proteins while the other areas can be passivated to prevent non-specific protein fouling. This is an interesting approach to develop biosensing platforms based on transparent, sustainable CNF nanopapers with convenient possibilities of orthogonal and self-reporting functionalizations. The transparency, the flat surface architecture and the high active surface area due to the presence of nanofibers may present advantages over e.g. using classical paper or also rather non-reactive plastic substrates. Additionally, the use of a simple inkjet printer to generate the pattern is important towards widespread use of the developed routines.

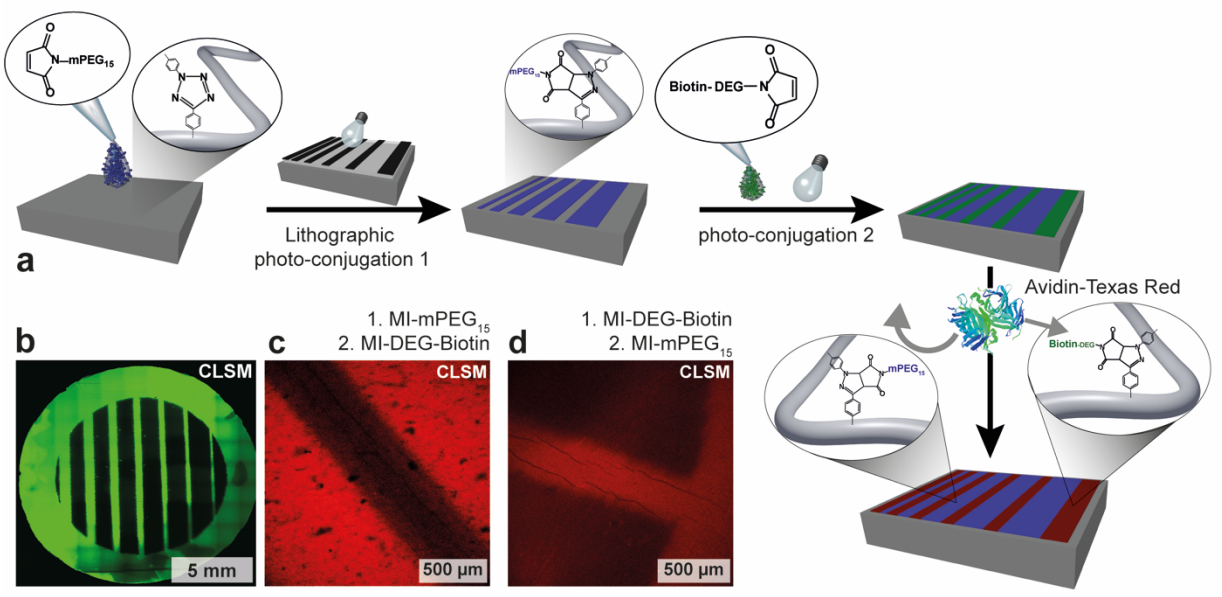

Figure 2. On-demand functionalization of transparent CNF-Tet nanopaper surfaces: (a) Schematic example of the patterning process to develop a biosensing film, starting with a lithographic photo-conjugation of PEG-maleimide by NITEC reaction to spatially prevent non-specific protein fouling, followed by a second photo-conjugation with biotin-DEG-maleimide as biorecognition moieties. In the last step, the florescent Avidin-Texas Red can bind to biotin, while the spatially resolved PEG stripes passivate against non-specific protein fouling (c). (b) CLSM of the spatially resolved photo-

patterned sample emphasizes the benefits of combining translucent cellulose nanopapers with the self-reporting feature of the NITEC reaction. (d) Reversing the routine reverses the functionality.

One of the emerging areas of nanocellulose research is the field of biomaterials where nanocellulose has become of interest as a fibrillar extracellular matrix to grow cells or tumor spheroids, as well as the use in additive manufacturing for 3D printing to make scaffolds for tissue engineering and tissue regeneration.[12-14, 16, 17, 20, 66-69] In all of these cases, it is very desirable to have additional degrees of freedom for controlling gelation externally and potentially even with spatial and temporal resolution. Therefore, we thought to combine freely flowing dispersions of CNF-Tet (0.4 wt%, 1.21 mM tetrazole units), which were previously modified with tetrazole units in dispersion, with a maleimide-capped star-PEG (sPEG-MI, 8 arms, $M_{n,star}$ = 10 kDa, 2.42 mM maleimide units) serving as multifunctional polymeric cross linker (Figure 3). Note that such star-PEGs are frequently used for biomaterials research and are known to be sufficiently biocompatible.[70-74] In terms of reaction partners, this corresponds to a two-fold excess of the maleimide over the tetrazole reaction partner. To follow the conjugation process, we first irradiated a small sample in a cuvette with 0.1 mm thickness and followed the development of the UV/Vis spectra (Figure 3c). The spectra undergo a clean change with a loss of absorption in the range of 300 nm (tetrazole), while a steady increase occurs in the range of ca. 375 - 425 nm, arising from the formation of the pyrazoline linkage. The spectra show a clear isosbestic point at ca. 330 nm, confirming a selective reaction, despite the fact that both reaction partners are immobilized either on a polymer or on colloidal nanofibrils.

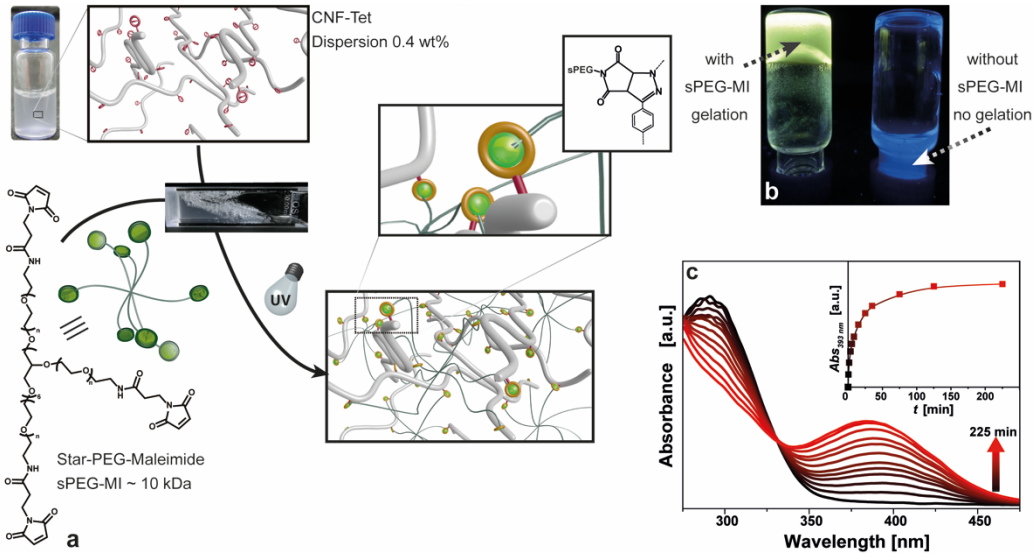

Figure 3. Photo-processable CNF hydrogels: (a) Scheme of the crosslinking for the preparation of a photo-induced CNF-Tet/sPEG-MI hydrogel by NITEC reaction. (b) The gel inversion test demonstrates

the transition of a flowing dispersion into a hydrogel network after 30 min irradiation, which corresponds to ca. 80% conversion as shown in the kinetic data, monitored by UV/Vis spectroscopy (c).

The reaction can be transferred to relevant volumes as shown in Figure 3b where a solid gel is obtained after UV irradiation of the CNF-Tet/sPEG-MI mixture, as shown by the gel inversion test. The gel is also highly fluorescent, confirming the successful occurrence of the self-reporting NITEC reaction. As a negative control, we also performed the same reaction in absence of sPEG-MI, which, as expected, does not allow gelation. This demonstrates that the physical state of CNF dispersions can be conveniently altered using photo-induced modular ligations with polymeric partners. Given the ample possibilities of functionalization of both the polymeric component and the CNF, the chemical and physical properties of the resulting gels can further be tuned for applications.

In addition to being relevant for modification of film-based applications and hydrogels as well as biomaterials, CNFs have also shown substantial promise for the engineering of high performance bioinspired nanocomposites, for which it is of utmost importance to control crosslinking reactions on a molecular level to promote fundamental understanding and target material advances in highly reinforced systems.[21, 63, 75-81] To this end, we mixed sPEG-MI (8 arms, $M_{n,star}$ =10 kDa) with a freely flowing CNF-Tet dispersion (0.25 wt%) and allowed these dispersions to evaporate to form solid films with different ratios of CNF/sPEG-MI (sPEG-MI = 0, 10, 20 and 50 wt%; Figure 4a). Subsequent irradiation with UV light (λ_{max} = 305 nm, ca. 6 mW cm^{-2}) using a mask leads to strongly fluorescent films at the non-masked region within seconds. Overall, the film remains translucent, but develops a yellowish tint (Figure 4b). The fluorescence confirms that the photo-induced conjugation can also take place in bulk state, despite the much lower dynamics compared to the dispersion and hydrogel state discussed above.

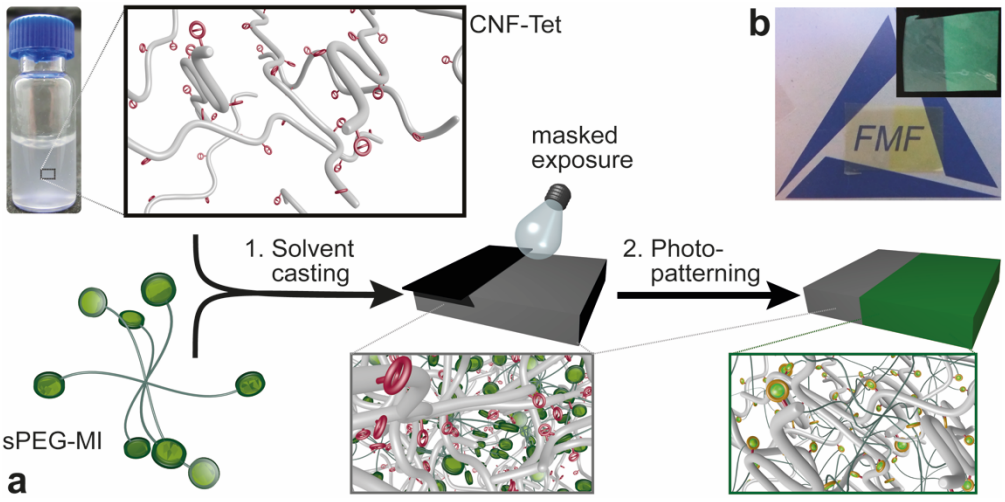

Figure 4. Photo-patterned crosslinking of CNF-Tet/sPEG-MI bulk materials. (a) Schematic representation of the film formation based on CNF-Tet and sPEG-MI by solvent casting and subsequent patterned crosslinking using a mask. (b) Patterned CNF-Tet/sPEG-MI (1/1 w/w) nanocomposite film after being exposed to UV-light with a mask, covering half of the film. The entire film remains translucent and a yellowish tint develops on the exposed right side. The inset shows the same film under irradiation with a 365 nm UV-hand lamp indicating a successful NITEC reaction in the nanocomposite.

To gain deeper insights, we monitored the reaction kinetics in a nanocomposite via UV/Vis spectroscopy (Figure 5d; 50 wt% sPEG-MI). A strong decrease at ca. 300 nm occurs with increasing reaction time, corresponding to the reaction of the tetrazole units, while the formation of a new peak at 375 to 400 nm is characteristic for the newly formed pyrazoline linkage. The evolution of the spectra shows a clear isosbestic point at ca. 330 nm, confirming a selective photo-conjugation even in the dry bulk nanocomposite state. Subsequently, we performed tensile tests to determine the influence of the crosslinking on the mechanical properties of the nanocomposites. Figure 5a displays the influence of the polymer content on the tensile properties of the composite nanopapers. Most importantly, the tensile curves show an increase in ductility and toughness upon incorporation of sPEG-MI. A softening is visible in a drop in stiffness and tensile strength. The strain-at-break shows a continuous extension up to $\varepsilon_b \approx 25\%$ upon incorporation of 50 wt% sPEG-MI (Figure 5a). The behavior originates from a toughening effect provided by frictional sliding of the CNFs enabled by intercalation of the soft polymer. This itself is a noteworthy result, because tailored toughening of CNF films is not straightforward to achieve.[27, 30, 76, 82, 83]

For the elucidation of the effect of photo-crosslinking on the mechanical properties, we focus entirely on the composite nanopapers containing 50 wt% sPEG-MI. Before irradiation, the films show a Young's modulus of $E \approx 1.6 \pm 0.2$ GPa, an ultimate strain-at-break of $\varepsilon_b \approx 25 \pm 5\%$ and an ultimate tensile strength of $\sigma_{UTS} \approx 56 \pm 2$ MPa. After UV irradiation, the films exhibit a distinct and very pronounced stiffening and strengthening. The stiffness and tensile strength roughly double to $E \approx 3.6 \pm 0.2$ GPa and $\sigma_{UTS} \approx 95 \pm 4$ MPa, while the strain-at-break is reduced to $\varepsilon_b \approx 11 \pm 1\%$ (Figure 5b). The stiffening demonstrates a successful covalent crosslinking of the nanocomposites and confirms the appearance of the self-reporting fluorescence on a molecular level (Figure 4b) to manifest in a change of macroscopic material properties. Accordingly, the corresponding micrographs of the fracture cross sections show a transition of the fracture behavior from a more tough to a stiffer material (Figure 5e-f). The non-crosslinked materials display a fuzzy and soft appearance with larger pull-out phenomena as originating from the soft non-crosslinked sPEG-MI, whereas, the crosslinked films reveal a more distinct roughness with less pull-out phenomena on larger length scale reminiscent of more brittle

fracture. We can compare the present results to Biyani et al.,[57] who used coumarin dimerization in adequately functionalized CNC-based composites within a rubber and found an increase of the stiffness by ca. 50% in dry state upon linking the CNC crystals together inside the rubber matrix. While one has to be careful with comparisons in the nanocellulose field due to non-standardized preparation methods, it becomes clear that the linkage of reinforcing segments with a multifunctional matrix, serving the crosslinking, is a powerful strategy toward mechanical strengthening, providing pathways to go beyond reinforcing percolation of fillers using covalent bonds.[1]

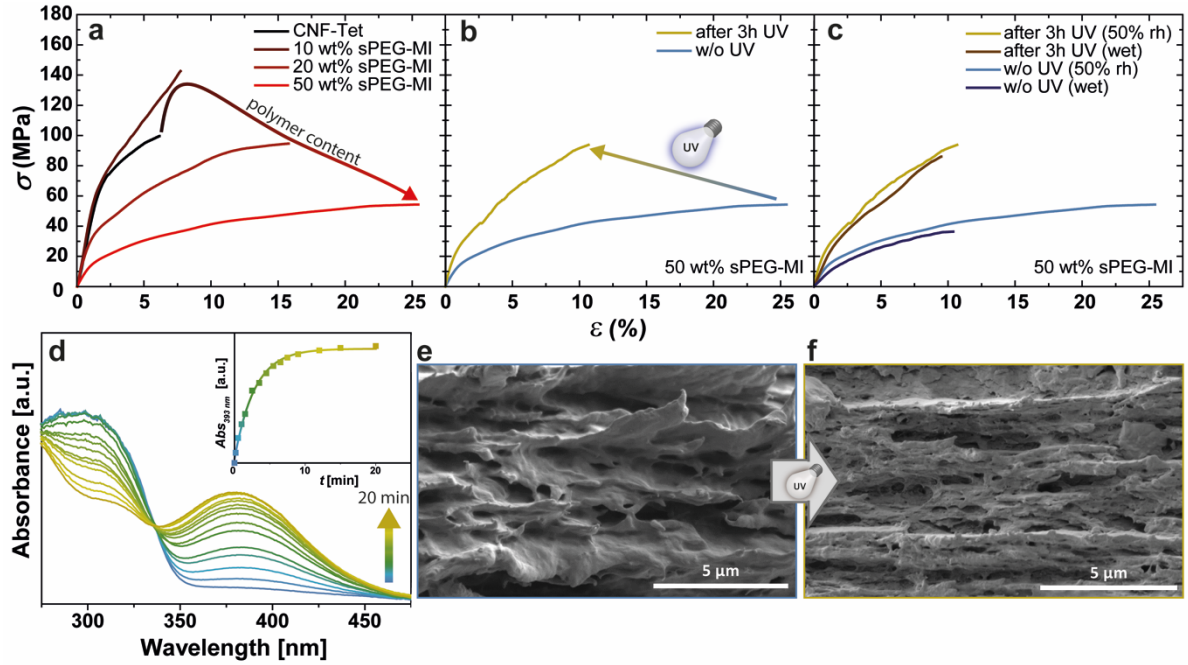

Figure 5. Characterization of photo-crosslinking of CNF-Tet/sPEG-MI nanocomposites: Tensile curves for (a) CNF-Tet with increasing content of sPEG-MI shows increasing toughness. (b) Stiffening effect after photo-induced crosslinking of a 1/1 w/w nanocomposite, (c) Comparison between a photo-crosslinked and non-crosslinked 1/1 w/w nanocomposite under wet conditions and standard conditions (50% relative humidity/rh). Gradient arrows are a guide to the eye to show the trends. (d) UV/Vis spectra of a CNF/sPEG-MI (1/1 w/w) nanocomposite film monitor the kinetic of the conversion with an isosbestic point at 330 nm. (e-f) Cross section micrographs of fractured nanocomposites with 50 wt% sPEG-MI of a non-crosslinked (e) and a crosslinked (f) film clearly show the transition of a ductile material with pull-out phenomena into a more brittle fracture stimulated by the photo-induced NITEC reaction.

Some of the most striking differences can be observed when immersing the samples into water and investigating their tensile properties in wet state (Figure 5c). Typically nanocellulose papers and also composite CNF/polymer nanopapers undergo considerable softening when prepared from water-soluble polymers.[24] For instance, plain CNF nanopapers of the herein used TEMPO CNF take up ca. 30 times their weight in water. Here, even the non-crosslinked CNF/sPEG-MI films only undergo moderate swelling (105% increase in weight), which is assisted by the

presence of the hydrophobic tetrazole units. However, a distinct softening occurs, as seen in the drop of stiffness and strength ($\varepsilon_b \approx 10 \pm 2\%$, $\sigma_{UTS} \approx 37 \pm 2$ MPa, $E \approx 0.8 \pm 0.2$ GPa), and more importantly, the material loses internal cohesion as the strain at break is considerably shortened to only half of the value measured in dry state (50%). The situation is different for the photo-crosslinked films. Those only undergo small swelling in water (68% increase in weight) and the mechanical properties of the dry state are almost fully maintained. Note that all values are normalized to the real thickness after immersion in water. This high level of mechanical stability after crosslinking is an encouraging result and highly sought after in functional and mechanical high-performance materials based on CNFs.

Conclusion

In summary, we established simple and fast functionalization protocols to equip CNFs in dispersion and in the bulk state with photoactive tetrazole units, and demonstrated their use for NITEC-based modular photo-ligation in three important material classes of different dynamics: photo-patterning of transparent nanopaper surfaces by exposure to liquid inks, light-triggered sol/gel transitions in hydrogels, and light-induced molecular engineering of mechanical properties in CNF/polymer bulk nanocomposites. The developed routines serve as self-reporting platform methods and open the door for applications in functional materials and devices. We herein particularly highlight the arising possibilities to change the mechanical properties of a nanocomposite material on-demand in a spatially resolved manner as demonstrated for the selective photo-crosslinking, and significant increase in stability in wet media. In future, more elaborate patterns can allow the generation of gradient materials that allow efficient stress delocalization and increased fracture resistance. Other relevant future approaches include multiplexing sensor assays on transparent nanopaper surfaces or the patterning of CNF-based hydrogel materials via lithography-based 3D printing technologies.

Conflicts of interest

There are no conflicts of interest to declare.

Acknowledgements

The authors acknowledge funding from the Deutsche Forschungsgemeinschaft (WA3084/7-1; BA 3751/35-1). C.B.-K. acknowledges continued support from the Queensland University of Technology (QUT) and the Australian Research Council (ARC) in the form of a Laureate Fellowship. C.B.-K. additionally acknowledges funding by the Karlsruhe Institute of

Technology (KIT) and the Helmholtz association via the BioInterfaces in Technology and Medicine (BIFTM), and the Science and Technology of Nanosytems (STN) programs.

References

1. A. J. Benitez and A. Walther, *J. Mater. Chem. A*, 2017, **5**, 16003-16024.
2. A. Barhoum, P. Samyn, T. Ohlund and A. Dufresne, *Nanoscale*, 2017, **9**, 15181-15205.
3. F. Jiang, T. Li, Y. Li, Y. Zhang, A. Gong, J. Dai, E. Hitz, W. Luo and L. Hu, *Adv. Mater.*, 2018, **30**, 1703453-n/a.
4. R. T. Olsson, M. A. Azizi Samir, G. Salazar-Alvarez, L. Belova, V. Strom, L. A. Berglund, O. Ikkala, J. Nogues and U. W. Gedde, *Nat. Nanotechnol.*, 2010, **5**, 584-588.
5. A. Liu, A. Walther, O. Ikkala, L. Belova and L. A. Berglund, *Biomacromolecules*, 2011, **12**, 633-641.
6. C. Eyholzer, A. B. de Couraca, F. Duc, P. E. Bourban, P. Tingaut, T. Zimmermann, J. A. Manson and K. Oksman, *Biomacromolecules*, 2011, **12**, 1419-1427.
7. T. Saito, R. Kuramae, J. Wohlert, L. A. Berglund and A. Isogai, *Biomacromolecules*, 2013, **14**, 248-253.
8. M. Wang, I. V. Anoshkin, A. G. Nasibulin, J. T. Korhonen, J. Seitsonen, J. Pere, E. I. Kauppinen, R. H. Ras and O. Ikkala, *Adv. Mater.*, 2013, **25**, 2428-2432.
9. H. Cai, S. Sharma, W. Liu, W. Mu, W. Liu, X. Zhang and Y. Deng, *Biomacromolecules*, 2014, **15**, 2540-2547.
10. Z. Shi, H. Gao, J. Feng, B. Ding, X. Cao, S. Kuga, Y. Wang, L. Zhang and J. Cai, *Angew. Chem. Int. Ed.*, 2014, **53**, 5380-5384.
11. K. Hua, D. O. Carlsson, E. Alander, T. Lindstrom, M. Stromme, A. Mihranyan and N. Ferraz, *RSC Adv.*, 2014, **4**, 2892-2903.
12. N. Lin and A. Dufresne, *Eur. Polym. J.*, 2014, **59**, 302-325.
13. J. G. Torres-Rendon, F. H. Schacher, S. Ifuku and A. Walther, *Biomacromolecules*, 2014, **15**, 2709-2717.
14. J. G. Torres-Rendon, T. Femmer, L. De Laporte, T. Tigges, K. Rahimi, F. Gremse, S. Zafarnia, W. Lederle, S. Ifuku, M. Wessling, J. G. Hardy and A. Walther, *Adv. Mater.*, 2015, **27**, 2989-2995.
15. H. Yagyu, T. Saito, A. Isogai, H. Koga and M. Nogi, *ACS Appl. Mater. Interfaces*, 2015, **7**, 22012-22017.
16. J. G. Torres-Rendon, M. Kopf, D. Gehlen, A. Blaeser, H. Fischer, L. De Laporte and A. Walther, *Biomacromolecules*, 2016, **17**, 905-913.
17. X. F. Yang, G. Q. Liu, L. Peng, J. H. Guo, L. Tao, J. Y. Yuan, C. Y. Chang, Y. Wei and L. N. Zhang, *Adv. Funct. Mater.*, 2017, **27**, 1703174-n/a.
18. H. Golmohammadi, E. Morales-Narvaez, T. Naghdi and A. Merkoci, *Chem. Mater.*, 2017, **29**, 5426-5446.
19. N. Halib, F. Perrone, M. Cemazar, B. Dapas, R. Farra, M. Abrami, G. Chiarappa, G. Forte, F. Zanconati, G. Pozzato, L. Murena, N. Fiotti, R. Lapasin, L. Cansolino, G. Grassi and M. Grassi, *Materials*, 2017, **10**, 977.
20. S. Sultan and A. Mathew, *Nanoscale*, 2018, DOI: 10.1039/c7nr08966j.
21. M. Wang, A. Olszewska, A. Walther, J. M. Malho, F. H. Schacher, J. Ruokolainen, M. Ankerfors, J. Laine, L. A. Berglund, M. Osterberg and O. Ikkala, *Biomacromolecules*, 2011, **12**, 2074-2081.
22. S. J. Eichhorn, *ACS Macro Lett.*, 2012, **1**, 1237-1239.

23. T. Saito, R. Kuramae, J. Wohlert, L. A. Berglund and A. Isogai, *Biomacromolecules*, 2013, **14**, 248-253.
24. A. J. Benitez, J. Torres-Rendon, M. Poutanen and A. Walther, *Biomacromolecules*, 2013, **14**, 4497-4506.
25. S. Fujisawa, T. Saito, S. Kimura, T. Iwata and A. Isogai, *Biomacromolecules*, 2013, **14**, 1541-1546.
26. M. Shimizu, T. Saito, H. Fukuzumi and A. Isogai, *Biomacromolecules*, 2014, **15**, 4320-4325.
27. A. J. Benitez, F. Lossada, B. Zhu, T. Rudolph and A. Walther, *Biomacromolecules*, 2016, **17**, 2417-2426.
28. N. Lavoine, J. Bras, T. Saito and A. Isogai, *Macromol. Rapid Commun.*, 2016, **37**, 1033-1039.
29. B. Wang, A. J. Benitez, F. Lossada, R. Merindol and A. Walther, *Angew. Chem. Int. Ed.*, 2016, **55**, 5966-5970.
30. A. J. Benitez and A. Walther, *Biomacromolecules*, 2017, **18**, 1642-1653.
31. Y. Liu, S.-H. Yu and L. Bergström, *Adv. Funct. Mater.*, 2017, DOI: 10.1002/adfm.201703277, 1703277.
32. C. Xu, O. Spadiut, A. C. Araujo, A. Nakhai and H. Brumer, *ChemSusChem*, 2012, **5**, 661-665.
33. I. Filpponen, E. Kontturi, S. Nummelin, H. Rosilo, E. Kolehmainen, O. Ikkala and J. Laine, *Biomacromolecules*, 2012, **13**, 736-742.
34. H. Hettegger, I. Sumerskii, S. Sortino, A. Potthast and T. Rosenau, *ChemSusChem*, 2015, **8**, 680-687.
35. K. S. Kontturi, K. Biegaj, A. Mautner, R. T. Woodward, B. P. Wilson, L.-S. Johansson, K.-Y. Lee, J. Y. Y. Heng, A. Bismarck and E. Kontturi, *Langmuir*, 2017, **33**, 5707-5712.
36. E. Lasseuguette, *Cellulose*, 2008, **15**, 571-580.
37. A. Isogai, T. Saito and H. Fukuzumi, *Nanoscale*, 2011, **3**, 71-85.
38. Y. Habibi, *Chem. Soc. Rev.*, 2014, **43**, 1519-1542.
39. Y. Zhang and O. J. Rojas, *Biomacromolecules*, 2017, **18**, 526-534.
40. S. Arola, T. Tammelin, H. Setala, A. Tullila and M. B. Linder, *Biomacromolecules*, 2012, **13**, 594-603.
41. H. Tang, N. Butchosa and Q. Zhou, *Adv. Mater.*, 2015, **27**, 2070-2076.
42. R. Weishaupt, G. Siqueira, M. Schubert, P. Tingaut, K. Maniura-Weber, T. Zimmermann, L. Thony-Meyer, G. Faccio and J. Ihssen, *Biomacromolecules*, 2015, **16**, 3640-3650.
43. H. Orelma, M. Vuoriluoto, L. S. Johansson, J. M. Campbell, I. Filpponen, M. Biesalski and O. J. Rojas, *RSC Adv.*, 2016, **6**, 85100-85106.
44. M. Dietrich, G. Delaittre, J. P. Blinco, A. J. Inglis, M. Bruns and C. Barner-Kowollik, *Adv. Funct. Mater.*, 2012, **22**, 304-312.
45. G. Delaittre, A. S. Goldmann, J. O. Mueller and C. Barner-Kowollik, *Angew. Chem. Int. Ed.*, 2015, **54**, 11388-11403.
46. H. Frisch, D. E. Marschner, A. S. Goldmann and C. Barner-Kowollik, *Angew. Chem. Int. Ed.*, 2018, **57**, 2036-2045..
47. J. S. Clovis, A. Eckell, R. Huisgen and R. Sustmann, *Chem. Ber.*, 1967, **100**, 60-70.
48. C. Rodriguez-Emmenegger, C. M. Preuss, B. Yameen, O. Pop-Georgievski, M. Bachmann, J. O. Mueller, M. Bruns, A. S. Goldmann, M. Bastmeyer and C. Barner-Kowollik, *Adv. Mater.*, 2013, **25**, 6123-6127.

49. P. Lederhose, Z. Chen, R. Müller, J. P. Blinco, S. Wu and C. Barner-Kowollik, *Angew. Chem. Int. Ed.*, 2016, **55**, 12195-12199.
50. R. K. V. Lim and Q. Lin, *Acc. Chem. Res.*, 2011, **44**, 828-839.
51. Z. Yu, T. Y. Ohulchanskyy, P. An, P. N. Prasad and Q. Lin, *J. Am. Chem. Soc.*, 2013, **135**, 16766-16769.
52. M. Zhou, J. Hu, M. Zheng, Q. Song, J. Li and Y. Zhang, *Chem. Commun.*, 2016, **52**, 2342-2345.
53. T. Tischer, C. Rodriguez-Emmenegger, V. Trouillet, A. Welle, V. Schueler, J. O. Mueller, A. S. Goldmann, E. Brynda and C. Barner-Kowollik, *Adv. Mater.*, 2014, **26**, 4087-4092.
54. A. Hufendiek, C. Barner-Kowollik and M. A. R. Meier, *Polym. Chem.*, 2015, **6**, 2188-2191.
55. A. Hufendiek, A. Carlmark, M. A. R. Meier and C. Barner-Kowollik, *ACS Macro Lett.*, 2016, **5**, 139-143.
56. H. Wondraczek, A. Kotiaho, P. Fardim and T. Heinze, *Carbohydr. Polym.*, 2011, **83**, 1048-1061.
57. M. V. Biyani, C. Weder and E. J. Foster, *Polym. Chem.*, 2014, **5**, 5501-5508.
58. M. V. Biyani, M. Jorfi, C. Weder and E. J. Foster, *Polym. Chem.*, 2014, **5**, 5716-5724.
59. J. Guo, W. Fang, A. Welle, W. Feng, I. Filpponen, O. J. Rojas and P. A. Levkin, *ACS Appl. Mater. Interfaces*, 2016, **8**, 34115-34122.
60. R. K. Johnson, A. Zink-Sharp and W. G. Glasser, *Cellulose*, 2011, **18**, 1599-1609.
61. Y. Okita, S. Fujisawa, T. Saito and A. Isogai, *Biomacromolecules*, 2011, **12**, 518-522.
62. S. Fujisawa, Y. Okita, T. Saito, E. Togawa and A. Isogai, *Cellulose*, 2011, **18**, 1191-1199.
63. K. Yao, S. Huang, H. Tang, Y. Xu, G. Buntkowsky, L. A. Berglund and Q. Zhou, *ACS Appl. Mater. Interfaces*, 2017, **9**, 20169-20178.
64. M. D'Este, D. Eglin and M. Alini, *Carbohydr. Polym.*, 2014, **108**, 239-246.
65. D. Hoenders, T. Tigges and A. Walther, *Polym. Chem.*, 2015, **6**, 476-486.
66. S. Shin and J. Hyun, *ACS Appl. Mater. Interfaces*, 2017, **9**, 26438-26446.
67. N. B. Palaganas, J. D. Mangadlao, A. C. C. de Leon, J. O. Palaganas, K. D. Pangilinan, Y. J. Lee and R. C. Advincula, *ACS Appl. Mater. Interfaces*, 2017, **9**, 34314-34324.
68. Y. Xue, Z. Mou and H. Xiao, *Nanoscale*, 2017, **9**, 14758-14781.
69. J. Wang, A. Chiappone, I. Roppolo, F. Shao, E. Fantino, M. Lorusso, D. Rentsch, K. Dietliker, C. F. Pirri and H. Grützmacher, *Angew. Chem. Int. Ed.*, 2018, **57**, 2353-2356.
70. E. A. Phelps, N. O. Enemchukwu, V. F. Fiore, J. C. Sy, N. Murthy, T. A. Sulchek, T. H. Barker and A. J. Garcia, *Adv. Mater.*, 2012, **24**, 64-70, 62.
71. M. V. Tsurkan, K. Chwalek, S. Prokoph, A. Zieris, K. R. Levental, U. Freudenberg and C. Werner, *Adv. Mater.*, 2013, **25**, 2606-2610.
72. T. Jungst, W. Smolan, K. Schacht, T. Scheibel and J. Groll, *Chem. Rev.*, 2016, **116**, 1496-1539.
73. J. S. Dudani, C. G. Buss, R. T. K. Akana, G. A. Kwong and S. N. Bhatia, *Adv. Funct. Mater.*, 2016, **26**, 2919-2928.
74. A. Shagan, T. Croitoru-Sadger, E. Corem-Salkmon and B. Mizrahi, *ACS Appl. Mater. Interfaces*, 2018, **10**, 4131-4139.
75. H. Sehaqui, Q. Zhou, O. Ikkala and L. A. Berglund, *Biomacromolecules*, 2011, **12**, 3638-3644.
76. H. Sehaqui, Q. Zhou and L. A. Berglund, *Soft Matter*, 2011, **7**, 7342-7350.
77. J. M. Malho, P. Laaksonen, A. Walther, O. Ikkala and M. B. Linder, *Biomacromolecules*, 2012, **13**, 1093-1099.

78. B. Zhu, N. Jasinski, A. Benitez, M. Noack, D. Park, A. S. Goldmann, C. Barner-Kowollik and A. Walther, *Angew. Chem. Int. Ed.*, 2015, **54**, 8653-8657.
79. B. Zhu, R. Merindol, A. J. Benitez, B. Wang and A. Walther, *ACS Appl. Mater. Interfaces*, 2016, **8**, 11031-11040.
80. H. Kargarzadeh, M. Mariano, J. Huang, N. Lin, I. Ahmad, A. Dufresne and S. Thomas, *Polymer*, 2017, **132**, 368-393.
81. J. Peng and Q. Cheng, *Adv. Mater.*, 2017, **29**, 1702959.
82. H. Jin, A. Y. Cao, E. Z. Shi, J. Seitsonen, L. H. Zhang, R. H. A. Ras, L. A. Berglund, M. Ankerfors, A. Walther and O. Ikkala, *J. Mater. Chem. B*, 2013, **1**, 835-840.
83. J. Yang and F. Xu, *Biomacromolecules*, 2017, **18**, 2623-2632.

Table of Contents

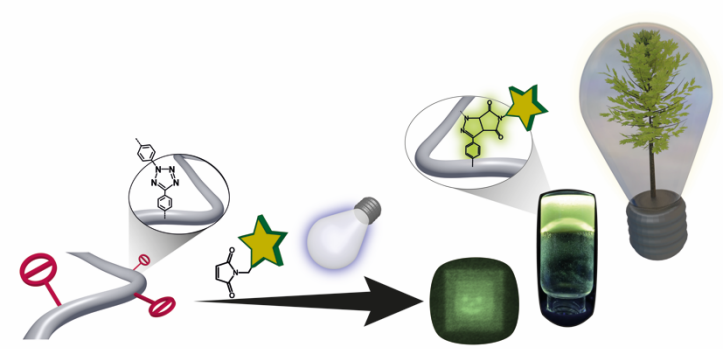

The fusion of tetrazole/maleimide-based photochemical ligation (self-reporting, selective) with cellulose nanofibrils (high mechanical properties, biocompatible, sustainable) establishes a versatile platform for bio-based advanced materials.